JOURNAL OF MATERIALS SCIENCE **35** (2000) 3505–3517

Effect of post-sintering heat-treatments on the erosive wear behaviour of liquid-phase-sintered aluminas

B. A. LATELLA*, B. H. O'CONNOR†
Materials Research Group, Department of Applied Physics, Curtin University of Technology, Perth, WA 6845, Australia
E-mail: bal@ansto.gov.au

The influence of microstructure on the indentation-strength and solid particle erosive wear behaviour of a liquid-phase-sintered (LPS) alumina subjected to coarsening, quenching and crystallisation heat-treatments were investigated. Strength as a function of crack size using Vickers indentations of varying loads was assessed. The short-crack toughness curves (T-curves) of the materials were evaluated from indentation-strength data which is pertinent to wear properties, since wear is governed by fracture characteristics at small flaw sizes. The effects of impact angle and particle velocity on erosive wear rates were also analysed. The relationship between short-crack toughness behaviour and erosion resistance are discussed with reference to the material microstructures and phase composition.

1. Introduction

Erosive wear constitutes a large problem for mining and mineral processing industries with large costs incurred from wear of material components. In response to this problem structural ceramics, particularly, liquid-phase-sintered (LPS) alumina ceramics, have been used as wear resistant liners for applications where ore bodies and slurries are transported, for example in transport chutes and pipelines [1]. These LPS aluminas have also enabled maintenance costs and downtime to be reduced in particular environments by their improved service performance compared to steels and polymers. Despite the popularity and widespread use of LPS aluminas as wear components, few studies have analysed both the short-crack T-curve response and erosive wear behaviour in terms of microstructural modifications.

Considerable effort has been devoted to enhancing the mechanical properties of alumina-based materials through microstructural tailoring [2–4]. However, little has been reported concerning the influence of microstructure and the characteristics of grain-boundary phases on erosive wear properties of these materials. Studies that have been reported varied widely in their conclusions [5–7].

Alternative approaches involving post-fabrication heat-treatments for strengthening of glass and glass-ceramics have been adapted to LPS aluminas to improve both the mechanical [8–10] and erosive wear properties [5]. There is, however, a deficiency in understanding the microstructural and compositional characteristics that govern whether pronounced increases in erosion resistance may be achieved through simple heat-treatments. The prospect of adjusting the mechanical and wear-resistant properties of LPS aluminas using simple post- sintering heat-treatments before placement in service is nevertheless quite appealing.

Crystallisation and quenching heat treatments have been used on LPS aluminas to (i) generate or minimise micro/macro stresses and (ii) manipulate the microstructure and phase assemblage [11]. Studies have indicated that quenching from high temperatures is effective in improving strength and toughness properties of LPS alumina ceramics [9, 11, 12]. Similarly, enhanced crystallisation or devitrification of grain-boundary glass is an approach that has been advocated and reported to improve toughness of this group of materials [9, 10, 12, 13]. These studies presumed single-valued toughness, precluding the detection of T-curve behaviour, and are therefore subject to scrutiny. An exception is the work by Zdaniewski and Kirchner [13], who measured toughness from crack size versus indentation load. In contrast, similar post-sintering heat-treatment studies of various LPS aluminas were shown to have little discernible effect on short-crack T-curve behaviour [8, 14, 15]. Furthermore, related attempts directed towards improving wear properties of alumina-based ceramics have yielded conflicting results adding to the considerable degree of controversy surrounding the benefits of post-sintering heat treatments and incorporating grain-boundary phases [5, 12, 16, 17].

* Now with the Materials Division, Australian Nuclear Science and Technology Organisation, PMB 1, Menai, NSW 2234, Australia.
† Author to whom all correspondence should be addressed.

Accordingly, in the present study, the T-curve behaviour and the erosion resistance of a low-cost LPS alumina, processed in-house complying to various design prescriptions [18] and subjected to a variety of heat treatments, has been investigated with emphasis on the individual and combined influences of grain size, nature of the grain-boundary phase and residual stress state. A pure alumina ceramic served as a control for comparative purposes. It is envisaged that the LPS alumina is to be used for specific erosion environments pertinent to the minerals processing industries within Western Australia.

The indentation-strength approach was used to evaluate the toughness behaviour of the materials in the domain of erosion crack sizes and a high velocity particle impact tester was employed for determining erosion rates. It is shown that contrary to some reports in the literature, the heat-treatments had only moderate effects on the strength properties, T-curve behaviour and erosion resistance. However, an apparent connection between toughness in the small-flaw domain and erosion performance was established.

2. Experimental procedure

2.1. Materials and characterisation

As indicated, the materials investigated were a pure alumina and a LPS alumina (nominally 85 wt.% α-Al_2O_3). Fabrication of these materials was via a conventional powder processing route as previously reported [19]. Specimens were prepared as disks ($\approx$22 mm diameter $\times$ 3 mm thickness) for indentation-strength tests and tiles (90 mm $\times$ 90 mm $\times$ 8 mm) for erosion tests. The pure alumina was chosen as a control for this work and also to distinguish the effect of grain size and composition on wear. The as-fired LPS alumina was subjected to a series of heat treatments to manipulate the microstructure and phase assemblage. The aims of the heat treatments were to: (i) recrystallise the intergranular phase without changing the grain size (HT-1), (ii) induce compressive surface stresses without changing the grain size (HT-2), (iii) increase the grain size (HT-3) and (iv) increase the grain size and induce compressive surface stresses (HT-4).

X-ray powder diffraction (XRPD) (Siemens D500) determined the nature and phase composition of the as-fired and heat-treated LPS aluminas from Rietveld analysis [20]. Scanning electron microscopy (SEM) (Phillips Jeol JSM-35C equipped with an EDS attachment) was used to examine the material microstructures. Grain sizes were determined using the linear intercept technique [21] on SEM images of polished and etched sections. Densities were measured by the Archimedes method using water as the immersion medium. The indentation hardness was evaluated as load/projected area from the impression diagonals of Vickers indentations using a contact load of 150 N and a fixed dwell time of 15 s. Young's modulus was determined for selected specimens using a non-destructive ultrasonic technique. Details of the heat-treatment schedules used and the absolute phase composition of the LPS materials are listed in Table I. The essential microstructure-property data of the high purity and LPS aluminas are summarised in Table II whilst the microstructures of the materials are shown in Figs 1 and 2.

2.2. Indentation-strength tests

Disk specimens were ground to about 2.5 mm thickness and polished on one side to a 1 μm finish. The polished surfaces were then indented at the face centre

TABLE I Description of post-sintering heat-treatment schedules for the LPS aluminas

Material designation	Heat-treatment process	Purpose	Phase structure	Composition (wt.%)
As-fired	—	—	α-Al_2O_3	86.7(1.4)[#]
			$MgAl_2O_4$	3.8(0.7)
			$CaAl_2Si_2O_8$	2.6(0.6)
			glass	6.9(1.6)
HT-1	1150°C, 24 h	Crystallise	α-Al_2O_3	86.5(1.4)
			$MgAl_2O_4$	5.4(0.7)
			$CaAl_2Si_2O_8$	8.6(0.7)
			glass	0.0(1.7)
HT-2	a) 1400°C, 1 h	Soak	α-Al_2O_3	87.2(1.4)
	b) Rapid air cooling from 1350°C to room temperature*	Quenching	$MgAl_2O_4$	2.9(0.7)
			$CaAl_2Si_2O_8$	1.5(0.6)
			glass	8.4(1.6)
HT-3	1500°C, 12 h	Grain-growth	α-Al_2O_3	89.7(1.4)
			$MgAl_2O_4$	2.1(1.1)
			$CaAl_2Si_2O_8$	2.0(0.6)
			glass	6.1(2.0)
HT-4	a) 1500°C for 12 h	Grain-growth	α-Al_2O_3	89.0(1.5)
	b) 1400°C for 1 h	Soak	$MgAl_2O_4$	2.4(1.1)
	c) Rapid air cooling from 1350°C to room temperature*	Quenching	$CaAl_2Si_2O_8$	2.1(0.6)
			glass	6.5(2.0)

[#]Standard deviations given in parentheses for most significant figures of value. Percent glass phase determined from: 100 - wt.% [alumina + spinel ($MgAl_2O_4$) + anorthite ($CaAl_2Si_2O_8$)].

*Rapid cooling ($\approx$2000°C/min) was achieved by transferring specimens from the furnace directly onto a thick steel block at room temperature (polished surfaces placed face down in contact with the steel plate) and convection cooling in a stream of air with a high velocity fan.

TABLE II Microstructural parameters and properties of the high-purity and LPS aluminas

Material	Density (g/cm^3)	Grain size/grain size range*	Hardness (GPa)	Natural strength (MPa)	Young's modulus (GPa)	Poisson's ratio
High-purity Al_2O_3						
Fine	3.91	2 / 1–5	18.0	594	340	0.19
Coarse	3.89	13 / 2–80	14.1	412	390	0.22
LPS Al_2O_3						
As-fired	3.56	4 / 1–6	12.0	454	270	0.23
HT-1	3.54	4 / 1–6	12.4	437	—	—
HT-2	3.57	4 / 1–6	11.9	475	—	—
HT-3	3.42	10 / 2–16	12.1	437	—	—
HT-4	3.43	10 / 2–16	12.1	401	—	—

*Approximate values of the smallest–largest grains in the material.

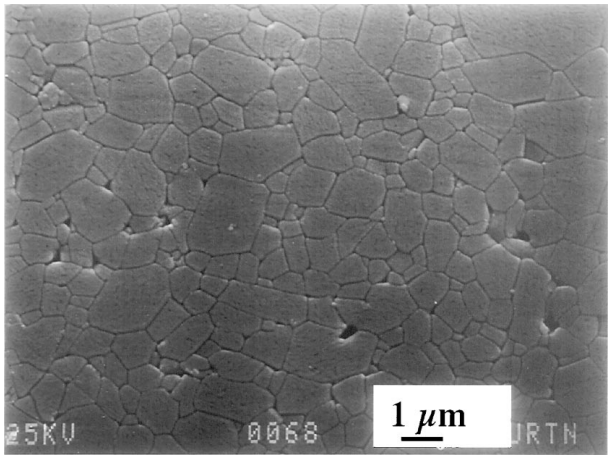

(a)

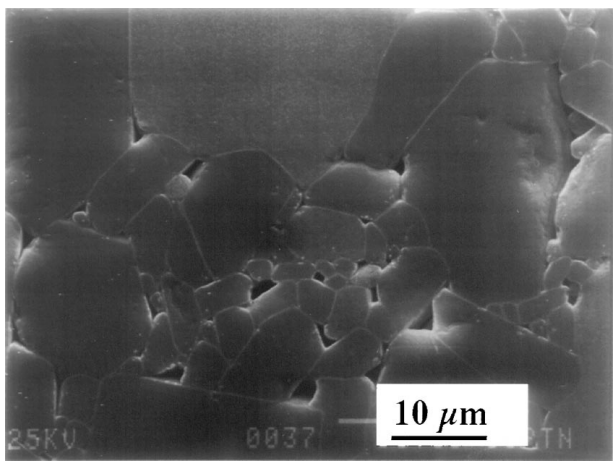

(b)

Figure 1 SEM (secondary electrons) micrographs of polished and thermally etched sections of (a) fine-grained and (b) coarse-grained alumina.

with a Vickers diamond indenter (Model 3212, Zwick) at contact loads $P = 3$ to 300 N. Some specimens were left unindented as controls. A drop of silicone oil was placed on the indentation site to minimise environmentally assisted subcritical crack growth prior to strength testing. The specimens were then broken in biaxial flexure using a screw-driven testing machine (Model 1122, Instron) at a fast loading rate (<20 ms break time) and the inert strengths determined. All broken specimens were examined to confirm failure initiation from the indentation sites. Specimens that did not fail from the indentation were omitted from the analysis.

The T-curve $T(c)$ with crack size c was deconvoluted from indentation-strength data using the technique developed by Braun *et al*. [22]. In a strength test with Vickers indentation cracks, the elastic-plastic residual contact stress intensity $K_R(c)$ supplements the applied tensile stress intensity $K_A(c)$ so that the net stress intensity is [23]:

$$K_N(c) = K_A(c) + K_R(c) = T(c) = \psi\sigma_A c^{1/2} + \frac{\chi P}{c^{3/2}} \quad (1)$$

where P is the indentation load, c is the crack length, ψ is a geometric parameter dependent upon crack shape and size, χ is the indentation contact-field coefficient and σ_A is the applied stress. For a material with single-valued toughness T_0, i.e. $T = T_0$, then $K_N = T_0$ in Equation 1, and $dT_0/dc = 0$, such that the fracture strength, σ_M, of the material is gven by:

$$\sigma_M = \frac{3}{4}\left(\frac{T_0^4}{4\psi^3\chi P}\right)^{1/3} \quad (2)$$

Thus, materials with single-valued toughness are characterised by a $P^{-1/3}$ dependence on σ_M. A shielding term $K_\mu(c)$ exists for ceramics with T-curve behaviour modifying Equation 1 to give:

$$K_N(c) = T_0 - K_\mu(c) = T_0 + T_\mu(c) = T(c) \quad (3)$$

where $T_\mu(c) = -K_\mu(c)$ is a shielding toughness term and $T(c)$ defines the T-curve for the material. Failure occurs for a given P, at the applied stress $\sigma_A = \sigma_M$ which satisfies the tangency conditions:

$$\frac{dK_N}{dc} = \frac{dT(c)}{dc} \quad (4)$$

It follows that T-curves are determined as the locus of tangency points to the family of $K_N(c)$ curves constructed from indentation-strength (σ_M,P) data sets. Accordingly, appropriate calibration of the coefficients ψ and χ in Equation 1 are required in order to construct the $K_N(c)$ curves. In this case, the calibrated coefficients used in deconvoluting the indentation-strength data of the aluminas, $\psi = 0.77$ and $\chi = 0.076$, were taken from data pertaining to a high-purity fine-

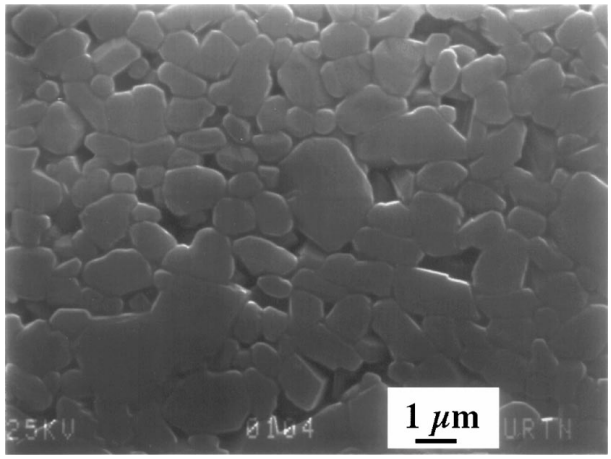

(a)

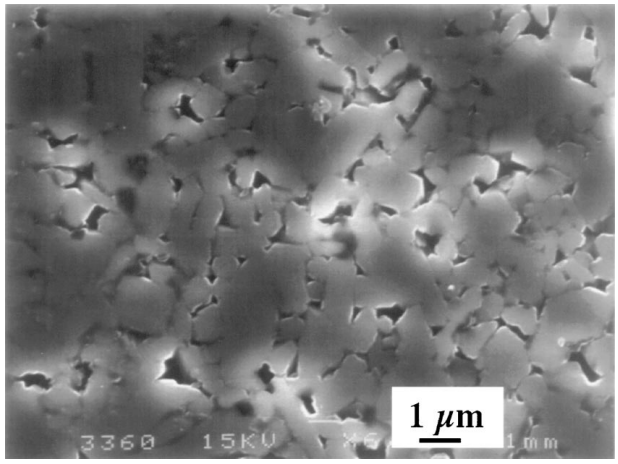

(b)

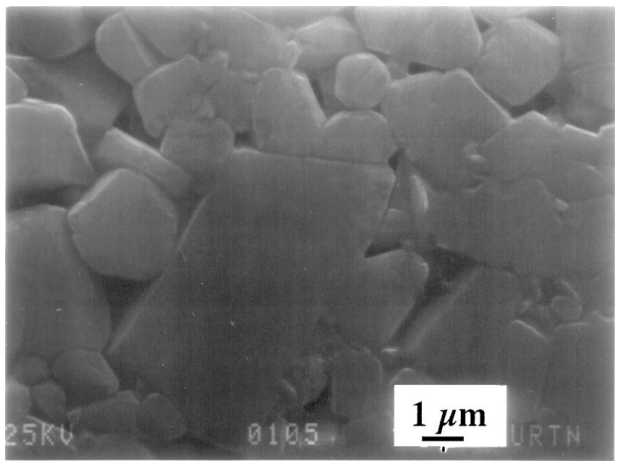

(c)

Figure 2 SEM (secondary electrons) micrographs of polished and thermally etched sections of (a) as-fired, (b) fine-grained crystallised (HT-1) and (c) coarse-grained (HT-3) LPS aluminas.

grained alumina with a grain boundary toughness $T_0 = 2.75$ MPa·m$^{1/2}$ [22]. For the LPS aluminas it was assumed that the crack geometry coefficient ψ is material-independent, so that $\psi = 0.77$ is retained and again using $T_0 = 2.75$ MPa·m$^{1/2}$. As a check some comparative Vickers indentation tests on the as-fired LPS alumina at various loads yielded an average toughness of 2.88 ± 0.23 MPa·m$^{1/2}$ [24] which compares favourably with the T_0 value given above and that obtained from the deconvoluted strength measurements (see later, Fig. 6). Allowing for a dependence in the residual contact field on the elastic modulus to hardness ratio $\chi \propto (E/H)^{1/2}$ (see Table II); $\chi = 0.078$ for the LPS alumina.

TABLE III Operating parameters of the erosion rig

Nozzle length	55 mm
Nozzle diameter	4 mm
Distance to sample	37 mm
Impingement angle	$\alpha = 20$–90°
Grit type	angular SiC
Grit size	270 μm median size
Air pressure	400 kPa
Grit velocity	$v = 95$ m/s

2.3. Erosion tests

Impact erosion was simulated by feeding a fixed mass of angular SiC grit into a high velocity air stream and then propelled through a WC nozzle onto the surface of the target specimen. Table III specifies the system parameters and operating range of the airborne particle erosion rig. Grit velocity was determined by the double rotating disk method [25].

The erosion trials were carried out over the range of impingement angles $\alpha = 20$–90°. Specimen tiles of each material, were cut into two equal halves and the prospective wear surfaces ground to a 10 μm surface finish. These were then ultrasonically cleaned, dried and weighed to 3 decimal place accuracy. Each specimen was placed in the erosion rig in turn and exposed to a fixed mass (200 g) of SiC grit in a test of approximately 40 s duration. The specimens were then re-washed in the ultrasonic bath to remove any residual SiC grit and dried in an oven. The dry mass of each specimen was recorded and the wear rate, W, determined as mass of the target material lost per unit mass of the incident erodent particles (mg/g). SEM observations were made on some eroded specimens to characterise the damage morphology. Both ultrasonically cleaned and as-eroded surfaces were utilised in the SEM examinations.

3. Results and discussion

3.1. T-curve behaviour

Fig. 3 shows inert strength versus indentation load results of the fine-grained (2 μm) and coarse-grained (13 μm) high-purity alumina control specimens. All data points with error bars on the plot represent the means and standard deviation limits of at least 4 specimens per load. The strengths of the materials based on breaks from natural flaws are indicated at the left axis by the shaded boxes. The solid straight line is the classical Griffith result for a material with a single-valued toughness (slope $= -1/3$). The data for the fine-grained alumina closely follow the solid line, indicative of a material with single-valued toughness. In contrast, the coarse-grained alumina exhibits a flattening in the strength-load response i.e. lower strength at low loads and enhanced strength at higher loads when compared with the fine-grained material.

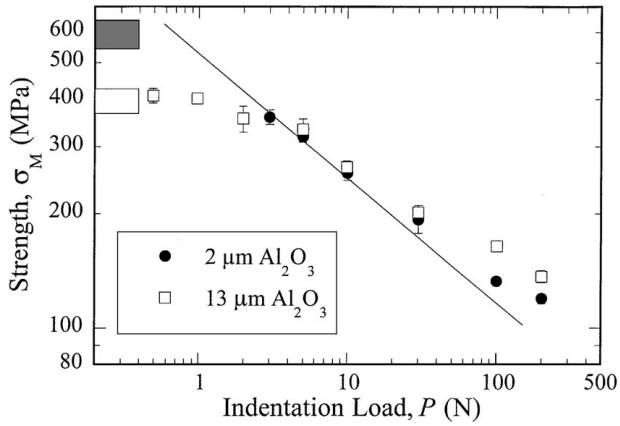

Figure 3 Plot of inert strength (σ_M) as a function of indentation load (P) for the fine- and coarse-grained high-purity aluminas. Shaded boxes at the left represent strength of the unindented specimens. Solid straight-line fit of slope −1/3 (logarithmic coordinates) is that for single-valued toughness ($T = T_0$).

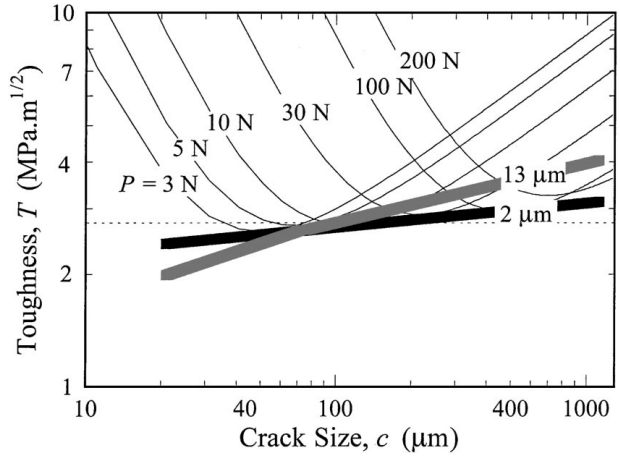

Figure 4 Deconvoluted T-curves for the fine- and coarse-grained high-purity aluminas using inert strengths σ_M at indentation loads P from Fig. 3. Dashed straight line represents single-valued toughness $T_0 = 2.75$ MPa·m$^{1/2}$.

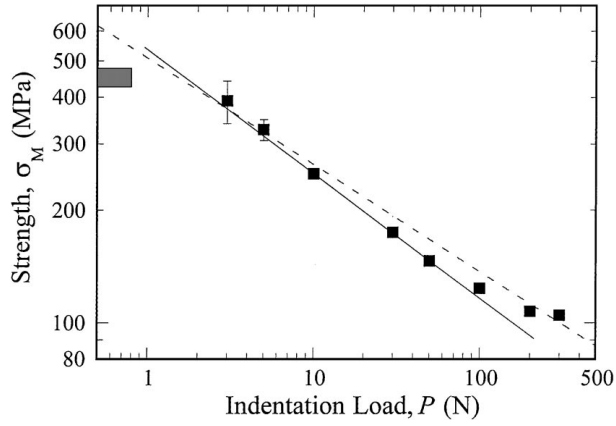

Figure 5 Plot of inert strength (σ_M) as a function of indentation load (P) for the as-fired LPS alumina compared with data from the fine-grained high-purity alumina represented by the best-fitted dashed line. Shaded box at the left represents strength of the unindented specimens. Solid straight-line fit of slope −1/3 (logarithmic coordinates) is that for single-valued toughness ($T = T_0$).

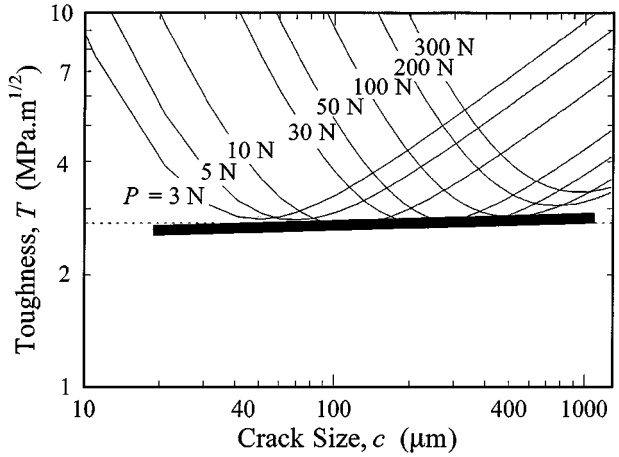

Figure 6 Deconvoluted T-curve for the as-fired LPS alumina using inert strengths σ_M at indentation loads P from Fig. 5. Dashed straight line represents single-valued toughness $T_0 = 2.75$ MPa·m$^{1/2}$.

The objective evaluation technique (Section 2.2) allowed construction of the short-crack T-curve diagrams for the aluminas from the strength data presented in Fig. 3. A family of "calibrated" $K_N(c)$ curves were constructed from each of the strength-load data points. The locus of tangency points through the data sets then determines the T-curve functions as shown in Fig. 4. The T-curves for the two materials intersect. For the fine-grained alumina, toughness remains essentially constant with increasing crack size, corresponding to the case where there is no microstructural shielding thus confirming its single-valued toughness. For the coarse-grained material the toughness rises with crack size. In the short-crack region (ca. $c < 100$ μm) the toughness of the coarse-grained alumina is lower than that of the fine-grained alumina but is greater in the long-crack region. The results show that scaling up the grain size is a principal element for flaw tolerance [23] attributed to enhanced T-curve behaviour [26], consistent with the work of other investigators. In the context of wear, the toughness value in the short-crack region is of particular importance as it corresponds to the region of micro-fracture controlled wear and consequently provides indications of erosion resistance characteristics.

Fig. 5 shows strength as a function of indentation load for the as-fired LPS alumina. Included for comparison is the best-fitted (dashed) line for the fine-grained high-purity alumina. The material exhibits Griffith-like behaviour with data points following the solid line except at large indentation loads where there is a strength plateau which is most likely due to lateral cracking [27]. As before, the family of curves in Fig. 6 was determined using the data from Fig. 5 to yield the fitted T-curve. In this instance the toughness coincides with the dashed horizontal line ($T_0 = 2.75$ MPa·m$^{1/2}$) for single-valued toughness.

Strength responses as a function of indentation load for the heat-treated LPS materials are shown in Fig. 7 along with the solid line representing a material with a constant fracture toughness. From the results in Fig. 7a there is a slight deviation and improvement in the strength at higher indentation loads for the HT-1 material relative to the solid line whereas the HT-2 data generally follow the solid line apart from the strength at $P = 100$ N which varied considerably as seen in the

experimental scatter for the data point. In Fig. 7b the indentation strength-load response of the HT-3 material exhibit slightly improved strength at higher indentation loads with no significant degradation in the strength at the low indentation loads. Likewise the HT-4 material demonstrated similar behaviour, with there being little measurable difference in the strength response apart from a greater degree of variability in the strengths at the large indentation loads compared with the HT-3 material.

The T-curves for each of the heat-treated materials are given in Fig. 8. The dashed line given in each plot is the assumed single-valued toughness value ($T_0 = 2.75$ MPa·m$^{1/2}$) of the materials. For the HT-1

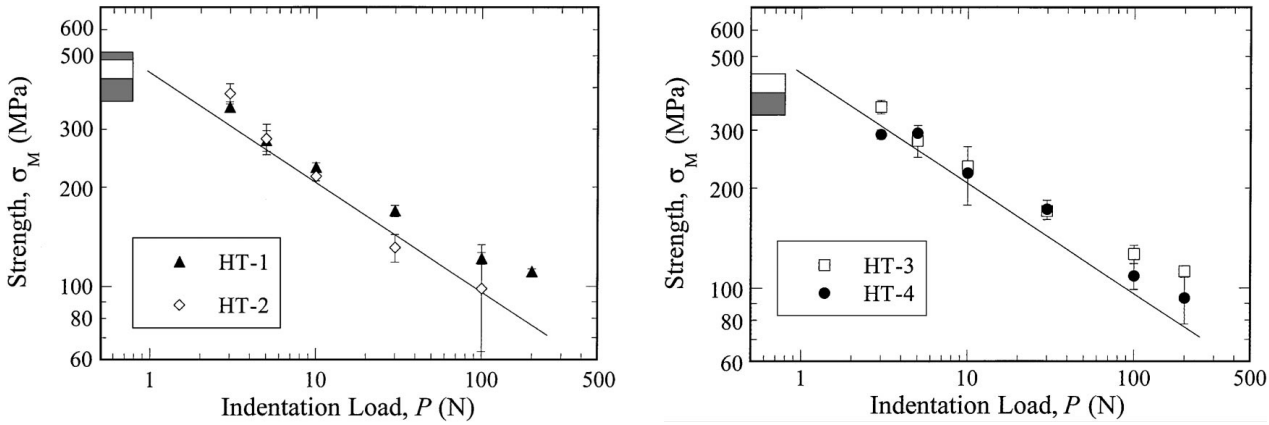

Figure 7 Plots of inert strength (σ_M) as a function of indentation load (P) for (a) the fine-grained crystallised (HT-1) and the fine-grained quenched (HT-2) LPS aluminas and (b) coarse-grained (HT-3) and coarse-grained quenched (HT-4) LPS aluminas. Shaded boxes at the left represent strengths of the unindented specimens. Solid straight-line fits of slope $-1/3$ (logarithmic coordinates) is that for single-valued toughness ($T = T_0$).

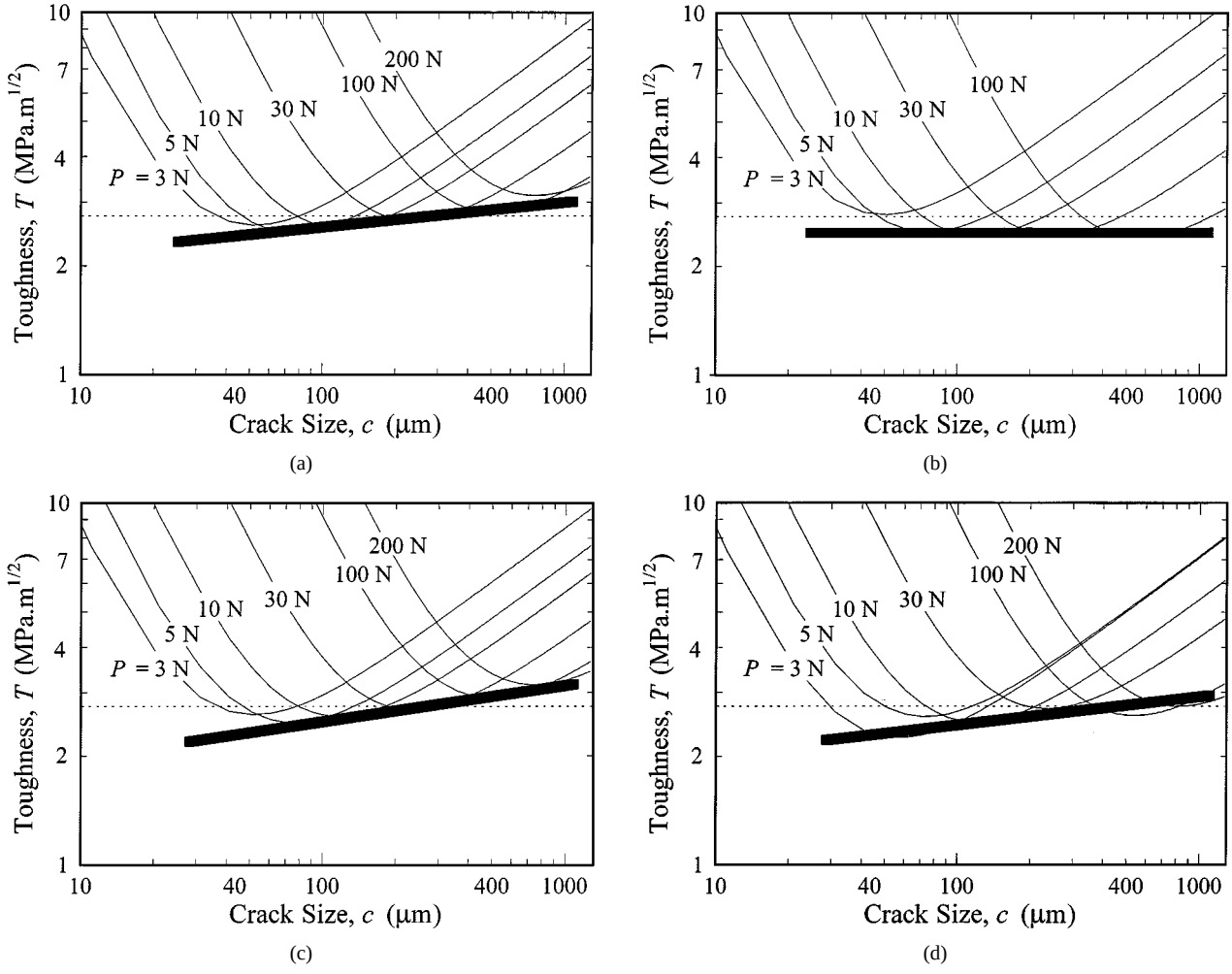

Figure 8 Deconvoluted T-curves for the (a) fine-grained crystallised (HT-1), (b) fine-grained quenched (HT-2), (c) coarse-grained (HT-3) and (d) coarse-grained quenched (HT-4) LPS aluminas. Shaded band is arbitrarily fitted T-curve and the dashed straight line represents single-valued toughness $T_0 = 2.75$ MPa·m$^{1/2}$.

material (Fig. 8a) the fitted T-curve exhibits a small rise with crack size. The T-curve for the HT-2 material (Fig. 8b) also conveys single-valued toughness although slightly lower than the assumed T_0 value. The HT-3 material (Fig. 8c) exhibits a slight T-curve as a consequence of the flattening in the strength-load response. This is also true for the HT-4 material (Fig. 8d).

The quantitative XRPD analysis for the heat-treated materials showed that specific changes in the concentrations of all the constituent phases occurred with heat treatment regime employed (Table I). The Rietveld calculations for the HT-1 material revealed that near 100% of the grain boundary glassy phase crystallised. As expected the quenching treatment (HT-2) resulted in a reduction of the amount of anorthite and spinel that crystallised from the glassy grain-boundary phase. An assessment of strain in the near-surface region of the quenched material using XRD (line broadening and line shift) indicated the presence of compressive uniform micro-strain effects. The coarsening treatments (HT-3 and HT-4) resulted in a higher α-Al_2O_3 matrix content and lower glass concentration intimating some precipitation of alumina from the glassy phase. Likewise, these materials exhibited lower anorthite and spinel concentrations compared with the as-fired LPS alumina.

It is clear that the thermal conditioning treatments to induce complete crystallisation of the glassy phase and quenching to develop compressive surface stresses in the LPS aluminas had only a minor effect on the strength and toughness properties. The presence of a small quantity of remnant glassy phase in the crystallised (HT-1) material could not be ruled out due to the uncertainty associated with the phase composition data, and as reported by others, is sufficient to relax induced stresses [14, 17]. Furthermore, crystallisation of the intergranular glass to anorthite and spinel appears to be inconsequential to strength properties. The quenching treatments (HT-2 and HT-4) are not adequate for the development of net surface compressive stresses as evidenced by increased variability in the strength data and signs of a toughness degradation in the HT-2 material. Coarsening of the microstructure resulted in a flattening in the strength-load response with a consequent rise in the T-curve, although too slight for any pre-failure stable crack growth. Hence, attempts to manipulate and control the nature of the grain boundary phase and residual stress state of the LPS alumina were shown to have relatively little effect on strength and toughness behaviour.

In view of the null-effect on the mechanical properties by air quenching, several as-fired LPS alumina specimens were rapidly cooled into a high viscosity silicone oil from 1350 °C. This treatment was more severe with all materials suffering from thermal shock, ruling out any indentation-strength or erosive wear analysis. However, some of these broken specimens were examined using direct crack size measurements as a function of Vickers indentation load (minimum of 5 indents per load) to evaluate the toughness [24] compared with the as-fired material which served as the control. Fig. 9a shows the mean crack lengths versus indentation load for the as-fired and oil-quenched

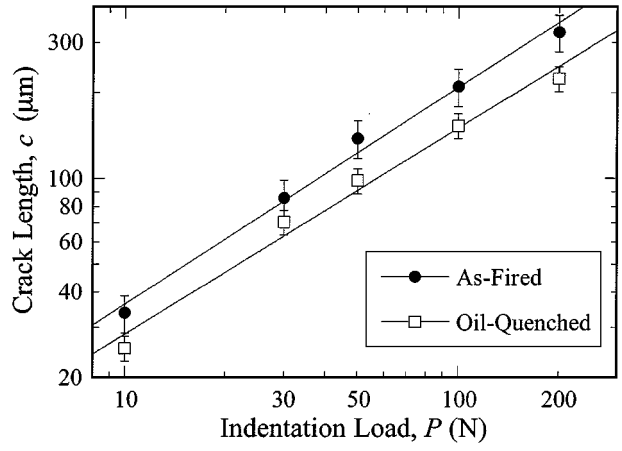

(a)

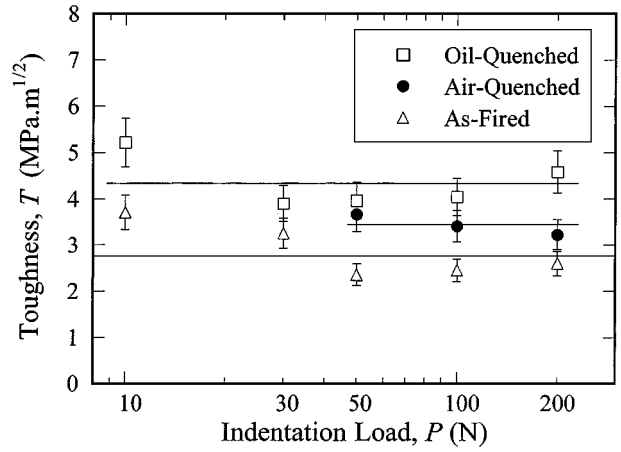

(b)

Figure 9 (a) Crack length as a function of indentation load for the as-fired and oil-quenched LPS aluminas with least squares fitted lines and (b) fracture toughness as a function of indentation load for the as-fired, air-quenched and oil-quenched LPS alumina.

materials. For any given indentation load, the radial crack lengths for the oil-quenched are smaller than the as-fired material, indicating a definite toughening response of the oil-quenched material. The toughness versus load plot in Fig. 9b shows this effect with about a 50% increase in the toughness of the oil-quenched (4.34 ± 0.26 MPa·m$^{1/2}$) to the as-fired material (2.88 ± 0.23 MPa·m$^{1/2}$). Included for comparison in Fig. 9b is the toughness data for the air-quenched material (3.43 ± 0.12 MPa·m$^{1/2}$), which shows an intermediate value between those of its as-fired and oil-quenched counterparts. Solid lines indicate the average toughness values. Note the difference in the toughness of the air-quenched material evaluated from deconvoluted strength measurements (2.44 MPa·m$^{1/2}$) to that obtained from Vickers–produced cracks. The reason for this discrepancy is unclear.

The toughening effect is rationalised in terms of the action of residual compressive stresses in opposing radial crack extension. This indicates the presence of net compressive surface stresses in the air- and oil-quenched materials. Using the toughness of the as-fired material ($K_c = 2.88$ MPa·m$^{1/2}$), an estimate of residual compressive stresses can be made from the radial crack lengths measured on quenched specimens assuming a uniform stress field [28], i.e. $K_c = \chi P/c^{3/2} + 2\sigma_r$

$(c/\pi)^{1/2}$ where σ_r is the residual stress and c is the crack length measured on the quenched material ($\chi = 0.078$). For the air-quenched material a compressive surface stress of $\sigma_r \approx 46$ MPa is obtained. It was established that the strength properties of the air-quenched material showed no discernible improvement over the as-fired material apart from increased variability in the data (Fig. 7a), indicating that the level of stresses induced is not sufficient to raise the contact damage threshold even though the toughness computed from direct crack size measurements is about 20% higher than the as-fired material. In contrast, oil quenching produces somewhat higher surface compressive stresses ($\sigma_r \approx 88$ MPa) which is expected to improve the contact damage threshold as indicated by the discernible toughness gain and demonstrated in quenching studies by others [9, 29, 30]. Ultimately, oil quenching is disadvantageous in that the LPS alumina suffers from thermal shock.

3.2. Erosive wear

3.2.1. Comparative erosion rates

The variation of erosion rate with impingement angle for the as-fired LPS alumina is shown in Fig. 10 along with the data for the fine- and coarse-grained high-purity aluminas. Each material exhibits minimal losses at low impingement angles, with monotonically increasing erosion rates to a maximum at $\alpha = 90^\circ$ which is characteristic of brittle behaviour.

The erosion rate of the coarse-grained alumina was higher over the angular range with the LPS alumina exhibiting the intermediate wear-resistance and the fine-grained alumina showing the most substantial wear-resistance. These differences in the erosion performance illustrate the importance of microstructure variation on wear susceptibility. It can be seen that increasing the grain size of the high-purity alumina has a significant influence on wear resistance with the coarse-grained high-purity alumina being about 3.5 times more susceptible to erosive wear than the fine-grained alumina. However, the LPS alumina portrays intermediate wear resistance between the aluminas even though it has a large ≈7 wt.% silicate glassy phase. This indicates that the alumina content and therefore glassy phase content is not always a reliable guide to wear performance [6] with other microstructural features, namely grain size, playing a significant role in erosive wear susceptibility [31]. Thus, in specific cases microstructural defects that initiate microcracking (e.g. grain size and porosity) may be more detrimental to erosion performance than those which aid in crack propagation (e.g. glassy grain boundary phases) [32].

The T-curve data support the erosive wear results as evidenced by the distinctly different short-crack toughness behaviour of the coarse-grained alumina to the fine-grained high-purity and as-fired LPS aluminas (Figs 4 and 6). The coarse-grained alumina displays rising T-curve behaviour, and degraded short-crack toughness, compared with the fine-grained high-purity alumina and the as-fired LPS alumina which both exhibit minimal T-curve characteristics. The improved strength and increased toughness in the long-crack region comes at the expense of reduced wear-resistance in the short-crack region [33]. Hence, the short-crack toughness value appropriate for the crack scales operative in erosion leads to better correlation with erosion results and the elastic-plastic erosion models [34, 35]. An estimate of the flaw size for the simplest "classical" case, i.e. $c = (K_c/\psi\sigma)^2$ (where $\psi = 2\alpha/\pi^{1/2}$) [36], for the as-fired LPS alumina ($\sigma = 454$ MPa, $K_c = 2.88$ MPa·m$^{1/2}$) yields a half-penny crack of radius $c \approx 25$ μm. This value provide a useful guide as to the approximate crack size region and hence the associated toughness applicable to erosive wear. As a consequence, T-curve behaviour provides a useful indicator of a material's susceptibility to wear, which is pertinent when selecting candidate materials for wear-related applications.

Fig. 11 presents the angular dependence of erosion rate (W) for the as-fired and heat-treated LPS aluminas. Included for comparison is the erosion response of a commercially available 85 wt.% alumina material (Coors AD85, elongated grain structure with ≈6 μm mean grain size). The angular response is equivalent to the trends shown in Fig. 10. Irrespective of the

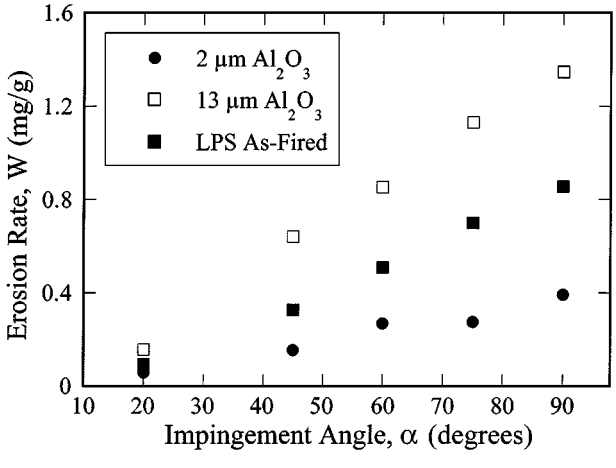

Figure 10 Erosion rate as a function of impingement angle for the as-fired LPS alumina and the fine- and coarse-grained high-purity aluminas.

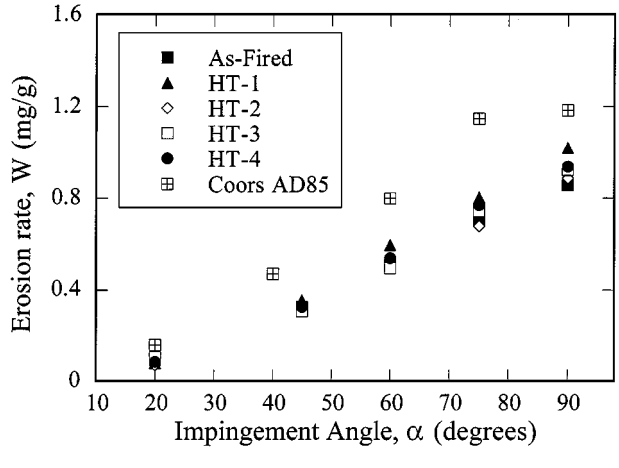

Figure 11 Erosion rate as a function of impingement angle for the as-fired and heat-treated LPS aluminas. Erosion data for a Coors AD85 alumina are included for comparison.

heat-treatment regime, all the materials exhibited similar erosion rates particularly at low angles with a tendency towards a greater degree of variability at higher impingement angles. A distinguishing feature is the lower erosion rates of the as-fired and heat-treated materials compared with the AD85 material. The key contributing factor for the superior erosion resistance of these materials compared to the commercial product is the tight control of the processing–microstructure link (powder processing, sintering regime, high density/low porosity, refinement of grain size and shape) employed to manufacture the materials examined in the present study [19]. Moreover, the effects of grain size and grain size distribution on erosion behaviour of a range of high-purity aluminas [37, 38] indicate that increasing the grain size does not necessarily lead to increased wear (refer to Appendix I for details). Evidently, detailed information of grain size distributions is as important as mean grain size when ascertaining the wear susceptibility of a material.

Crystallisation of the grain-boundary glassy phase appears to have a modest influence on erosion performance, exhibiting slightly higher erosion rates of the treated materials at 60–90°. Moreover, the microstructural coarsening and/or quenching treatments showed no obvious improvement or degradation in erosion performance when contrasted with the as-fired material.

It would be expected that the erosion performance of the coarsened materials (HT-3 and HT-4) would be considerably degraded in comparison to the fine-grained as-fired LPS alumina, likened to the wear behaviour of the high-purity alumina, although this was not the case. This may be due to the narrow grain size distribution of the coarsened materials adding further support to the erosion results obtained for the high-purity aluminas (Appendix I). The apparent anomaly could also be attributed to the higher α-Al_2O_3 content ($\approx$3 wt.%) in the HT-3 and HT-4 materials compared with the as-fired control (see Table I). Although inconclusive, the increase in grain size may be somewhat counterbalanced by the moderate increase in α-Al_2O_3 content in their combined effect on erosion. Overall, the erosion results highlight the apparently less damaging effect of coarsening the grain size of the heat-treated LPS aluminas (Fig. 11) when compared with the equivalent high-purity aluminas which showed an extreme grain size–wear sensitivity (Fig. 10).

The relationship between erosion rate (W) and $v \sin\alpha$ (normal component of velocity), expressed as $W \propto (v \sin\alpha)^n$ on a logarithmic scale is shown in Fig. 12 for the as-fired and HT-1 LPS alumina specimens and the fine- and coarse-grained high-purity aluminas. A least-squares fit was made through the data, and the value of the slope of the least-squares line is reported as the velocity exponent, n. The velocity exponents of all the specimens tested are presented in Table IV. These velocity exponents are lower than the values asserted by the models [39, 40], which may be expected because the exponent depends critically on particle geometry, interactions with the surface and details concerning the scaling law used to relate fracture mechanics to material removal [41]. Hence, the variations in the experimentally determined velocity exponents, particularly for the heat-treated material, is attributed to the complex nature

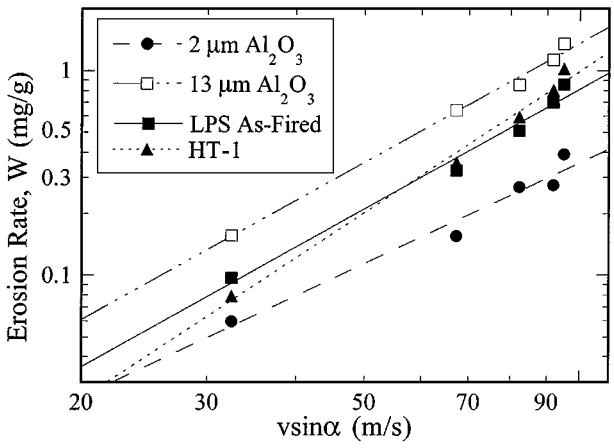

Figure 12 Logarithmic plot of erosion rate as a function of the normal component of velocity for the fine- and coarse-grained high-purity aluminas and the as-fired and HT-1 LPS aluminas. The lines represent the linear least squares fit through the data points for each material.

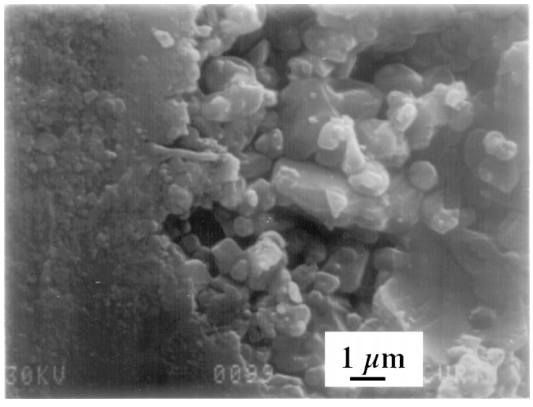

(a)

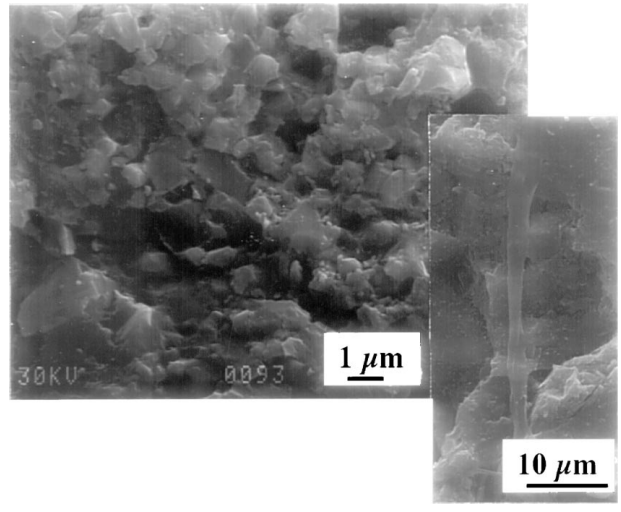

(b)

Figure 13 Erosive wear zone images of the as-fired LPS alumina at impingement angles of (a) 20° and (b) 90° (inset: area showing localised melting; note stringy morphology).

of the multi-particle impacts. Various studies [32, 42] have attempted to relate these differences in velocity exponents to transitions in material removal mechanisms. For the as-fired and heat-treated LPS aluminas no such distinction could be made due to overlap in the relative uncertainties of the velocity exponents. However, the fine- and coarse-grained high-purity aluminas display measurable differences in the velocity exponents which appears to be associated with distinctive erosion failure mechanisms (see Section 3.2.2). The main conclusion drawn from the data presented in Table IV is that a value of $n \approx 2$ for the damage process is essentially proportional to the normal component of the kinetic energy of the SiC erodent particles.

TABLE IV Velocity exponents of the high-purity and LPS aluminas

Material designation	Velocity exponent, n
Fine-grained Al_2O_3	1.6(1)[#]
Coarse-grained Al_2O_3	1.93(8)
As-fired LPS Al_2O_3	2.0(2)
HT-1	2.3(1)
HT-2	2.2(1)
HT-3	1.9(2)
HT-4	2.1(1)

[#]Standard errors of the mean (95% confidence interval) for the least significant digit are given in parentheses.

3.2.2. Microstructural damage

Representative SEM micrographs of the erosion surfaces for the as-fired LPS alumina at impingement angles of 20° and 90° are shown in Fig. 13. At low impingement angles, the damage in the material is characterised predominantly by scratching and microfracture processes (Fig. 13a). By contrast, at high impingement angles (Fig. 13b) there is a greater degree of damage with material removal in these instances dominated by intergranular cracking and chipping. There is also evidence of some grain dislodgment and material fall-out with obvious cavities visible due to preferential wear of the grain boundary glassy phase.

In various eroded regions of the as-fired LPS alumina specimens examined, long thin stringy forms were apparent. Energy dispersive spectrometry (EDS) analysis of these stringy structures revealed the presence of Si, Mg and Ca, the major elements of the glassy phase [19], as well as Al, indicating localised melting of the glass phase. The inset in Fig. 13(b) shows the solidified remnant produced in the melting of the glassy phase by the solid particle impact. An idealised model [43] was

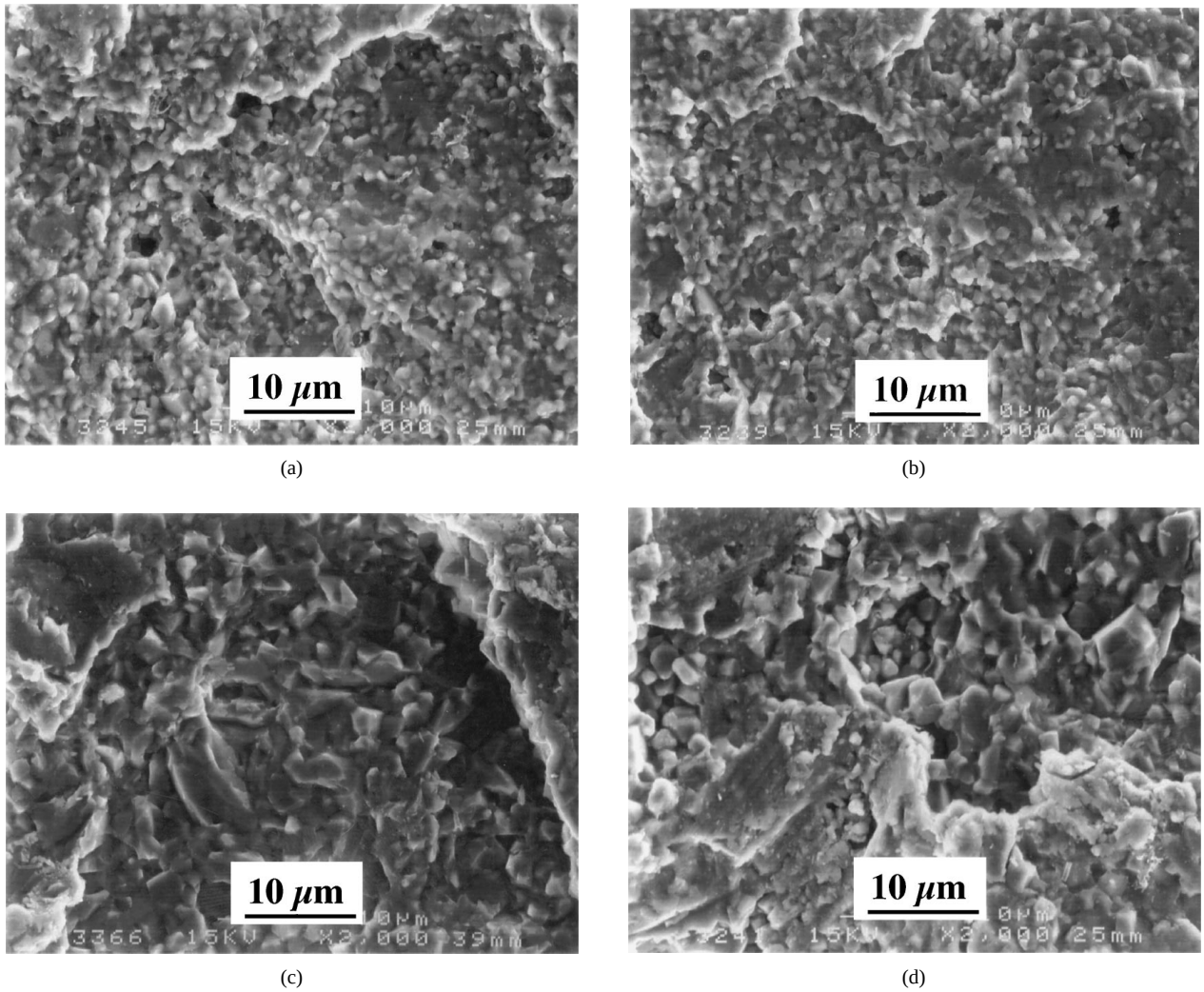

(a) (b) (c) (d)

Figure 14 Erosive wear zone images of (a) fine-grained crystallised (HT-1), (b) fine-grained quenched (HT-2), (c) coarse-grained (HT-3) and (d) coarse-grained quenched (HT-4) LPS aluminas at impingement angles of 90°.

used to gain an estimate of the temperature increase in an impact event. The temperature change determined was ≈1140 °C, which is higher than the softening temperature of the grain boundary glassy phase and approaching the melting point of the glass (1190 °C) [19], confirming that melting is quite likely to occur. Nevertheless, SEM examinations of eroded surfaces show that the melting process occurs sparingly but in a random manner, thus depending on the contact conditions.

As expected, from the erosive wear data (Fig. 11), the wear damage areas of the heat-treated materials were found to be generally comparable to the as-fired LPS alumina with the same material removal processes operable. Typical erosion surfaces of the fine-grained crystallised (HT-1), fine-grained quenched (HT-2), coarse-grained (HT-3) and coarse-grained quenched (HT-4) LPS aluminas at 90° impact are shown in Fig. 14. Intergranular cracking is predominant in the fine-grained materials (HT-1 and HT-2) along with evidence of small cavities resulting from grain ejection. There are some slight differences in the damage mechanisms in the coarsened materials (HT-3 and HT-4) with transgranular fracture, chipping and cleavage of grains increasingly more evident.

The erosion surfaces of the fine- and coarse-grained high-purity aluminas portrayed some obvious differences in the damage mechanisms compared with the LPS aluminas. SEM micrographs of the surfaces eroded at an impingement angles of 20° and 90° for the fine- and coarse-grained materials are shown in Figs 15 and 16, respectively. At low impact angles, the fine-grained material showed scratching, scarring and flaking (Fig. 15a) whereas at high impact angles extensive grain-boundary chipping became evident (Fig. 15b). By contrast, the coarse-grained high-purity alumina showed little evidence of inelastic deformation and scratching with material removal being controlled by transgranular and intergranular chipping and grain dislodgment (Fig. 16). Consequently, the coarse-grained material did not exhibit any such transition in damage mode apart from an increase in severity of the transgranular and intergranular chipping processes.

It was recognised from the values of the velocity exponents given in Table IV that there may indeed be a link with erosion failure mechanism. Clearly the differences in the respective wear modes of the fine- and coarse-grained high-purity aluminas, principally at low impingement angles, alludes to such a link but is somewhat less convincing at high impingement angles. Nevertheless, the discrepancy in the velocity exponents may be associated with: (i) an increased efficiency in the grain-boundary removal mechanism in the

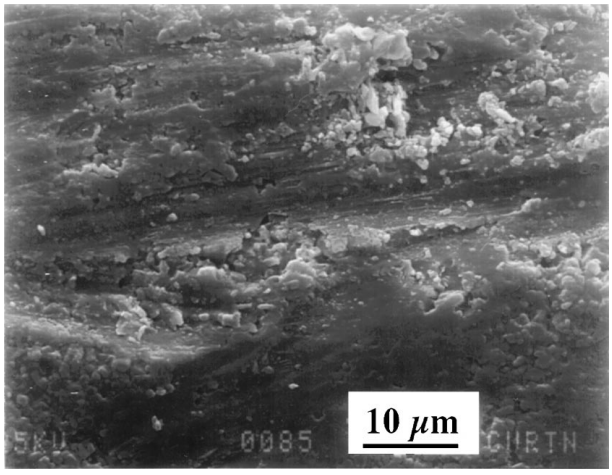

(a)

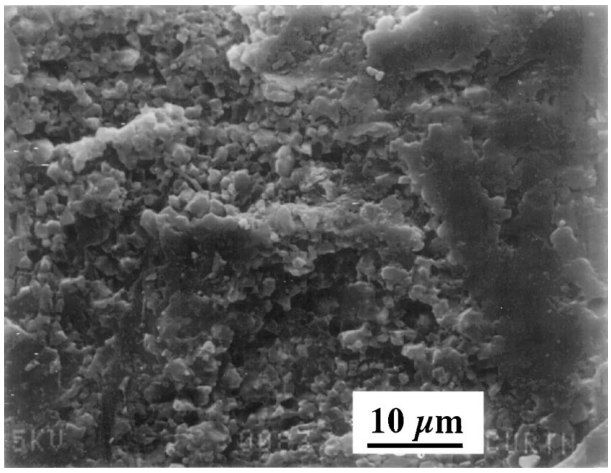

(b)

Figure 15 Erosive wear zone images of the fine-grained high-purity alumina at impingement angles of (a) 20° and (b) 90°.

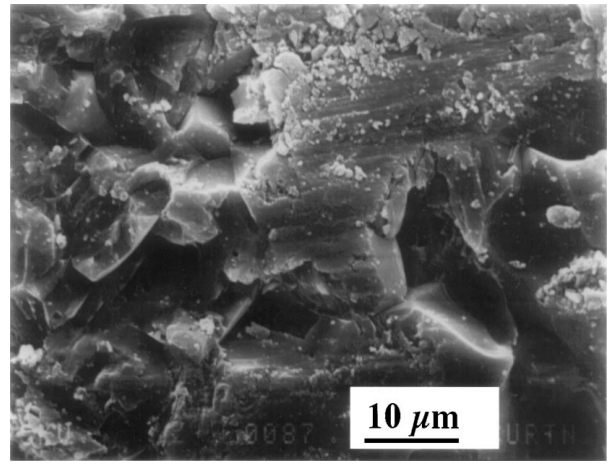

(a)

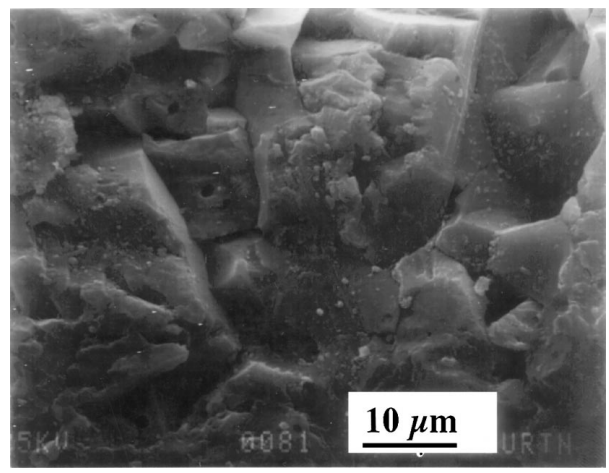

(b)

Figure 16 Erosive wear zone images of the coarse-grained high-purity alumina at impingement angles of (a) 20° and (b) 90°.

coarse-grained alumina which is supported by erosion rate data and SEM damage evaluations or (ii) an erodent particle size/target grain size effect in which the velocity exponent decreases as the ratio of the particle size to target grain size is increased [32].

4. Conclusions

The principal conclusions from the study are as follows:

1. The indentation-strength tests performed on the LPS aluminas provided clear evidence of the effects of post-sintering heat-treatment and offered a means of evaluating T-curve behaviour especially in the realm of the short-crack region which is pertinent to wear.

2. The nature of the intergranular second phase and the specific post-sintering heat treatments, had no appreciable effect on the strength or T-curve properties of the LPS aluminas examined in this work.

3. The erosion results supported the strength and toughness findings, there being no discernible change in wear performance as a consequence of the heat-treatments. The crystallised material (HT-1) appeared to show signs of increased erosion rates at high impingement angles attributable to induced stresses derived from thermal expansion mismatch between the alumina matrix and the crystallised phases [44]. In contrast, the quenching treatments of the fine- and coarse-grained LPS aluminas, HT-2 and HT-4, respectively, had no effect on erosion performance. The erosion response of the coarsened materials (HT-3 and HT-4) generally matched that of the as-fired LPS alumina contrary to expectations of greater wear susceptibility. Contrary to the high-purity alumina which showed an appreciable increase in wear with increase in grain size, coarsening the LPS alumina revealed little deleterious effect on wear rate.

4. The relative importance of grain size and purity (phase composition) on erosion rate in the LPS and high-purity aluminas was demonstrated. The coarse-grained high-purity alumina showed significantly higher erosion rates compared to its fine-grained counterpart and the as-fired (fine-grained) LPS alumina which showed intermediate wear resistance even though it has a large secondary phase.

5. The erosion rates of the as-fired and heat-treated LPS aluminas were found to be proportional to the kinetic energy of the impinging particles according to the velocity exponents. Microstructural damage studies of the LPS aluminas revealed that surfaces eroded at 20° showed abrasive scratching and ploughing. Observations of the damage sites in the LPS and high-purity aluminas eroded at 90° confirmed that material removal occurs by a brittle mechanism consistent with the characteristic angular dependence of brittle materials. Erosion processes in the LPS aluminas consists of repeated deformation, cutting and material removal by intergranular fracture whereas the dominant mechanism of material removal in the high-purity aluminas is intergranular fracture.

In the context of the study, the LPS alumina is considered appropriate for use as erosive wear liners given the improved wear performance over similar commercial materials and the low cost of fabrication. The LPS alumina is especially suited for large volume problem wear environments which exist in the minerals processing industries. Moreover, subjecting this material to various heat-treatments has shown that the strength, flaw tolerance properties and erosion performance are not significantly affected i.e "heat-treatment tolerant". Nonetheless, the benefits of the null effect have important implications in materials processing and utilisation in environments where contact damage and erosion resistance are controlling factors. The capacity of the material to tolerate thermal fluctuations and the insensitivity of the properties to these changes may lead to potential applications.

Appendix I

Two grades of high-purity aluminas, both with fine- and coarse-grained microstructures [38, 45], were examined to ascertain the effects of grain shape and grain size distribution on erosion rate. The essential characteristics of the materials are as follows:

(i) **Fine-N** (fine-grained, narrow grain size distribution): alumina sintered at 1600°C for 5 h from a high-purity alumina powder (AKP-50, Sumitomo) with mean grain size of 5 μm, equiaxed grains and narrow grain size distribution (smallest grains 1–2 μm, largest grains 15–18 μm).

(ii) **Fine-B** (fine-grained, broad grain size distribution): alumina sintered at 1600°C for 5 h from a high-purity alumina powder (A-16SG, Alcoa) with mean grain size of 4.0 μm, equiaxed grains and broad grain size distribution (smallest grains 1 μm, largest grains 20–25 μm).

(iii) **Coarse-N** (coarse-grained, narrow grain size distribution): alumina sintered at 1700°C for 25 h from a high-purity alumina powder (AKP-50, Sumitomo) with mean grain size of 10.2 μm, equiaxed grains and narrow grain size distribution (smallest grains 2–5 μm, largest grains $\approx$30 μm).

(iv) **Coarse-B** (coarse-grained, broad grain size distribution): alumina sintered at 1700°C for 25 h from a high-purity alumina powder (A-16SG, Alcoa) with mean grain size of 12.8 μm, equiaxed grains and broad grain size distribution (smallest grains 2–5 μm, largest grains $\approx$75 μm).

Fig. A1 shows the comparative erosion rates of the four materials at an impact angle of 90° under the same conditions as described in Section 2.3. It is apparent that doubling the grain size of the narrow grain size distribution materials (Fine-N and Coarse-N) has only a minimal effect on the comparative erosion rates. In contrast the wear rate of the Coarse-B (broad grain size distribution) material is about 50% greater than Coarse-N. Clearly, even though Fine-N and Fine-B as well as Coarse-N and Coarse-B essentially have equivalent mean grain sizes, the disparity in wear rates can be attributable to differences in the grain size distributions. Hence, simply reporting mean grain size may not

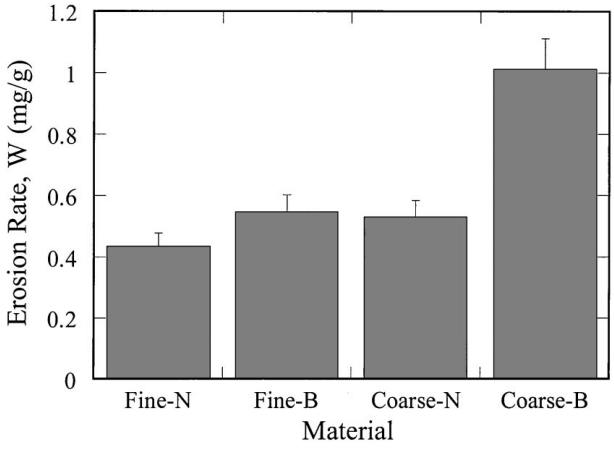

Figure A1 Comparative erosion rates for the Fine-N, Fine-B, Coarse-N and Coarse-B high-purity aluminas at an impingement angle of 90°.

always provide a true indication of the overall microstructural traits and accordingly relating it to the material's wear susceptibility. It appears from the experimental data presented here that knowledge of the grain size distribution provides further critical information that can be helpful in the analysis of the wear behaviour of materials.§

Acknowledgements

This work was partly funded by the Minerals and Energy Research Institute of Western Australia (MERIWA) (Project M207). The authors acknowledge Dr. B. R. Lawn of the National Institute of Standards and Technology for supporting part of this work and Dr. D. Kovar of the University of Texas for helpful discussions and supplying some high-purity aluminas used in the study.

References

1. A. M. MACDONALD, P. J. MUTTON and W. J. SINCLAIR, "Abrasion Resistant Materials for the Australian Minerals Industry, Vol. 2: Applications for Advanced Ceramics" (Australian Mineral Industries Research Association, Melbourne, 1988).
2. P. CHANTIKUL, S. J. BENNISON and B. R. LAWN, *J. Am. Ceram. Soc*. **73** (1990) 2419.
3. S. J. BENNISON, N. P. PADTURE, J. L. RUNYAN and B. R. LAWN, *Philos. Mag. Lett.* **64** (1991) 191.
4. N. P. PADTURE, S. J. BENNISON and H. M. CHAN, *J. Am. Ceram. Soc*. **76** (1993) 2312.
5. E. Y. GUTMANAS, N. A. TRAVITZKY, N. A. STONE and A. I. KINGON, *Mater. Sci. Eng*. **96** (1987) L5.
6. G. R. HEATH, T. D. JOHNSON, M. T. PARRY and D. J. WALL, *Trans. J. Brit. Ceram. Soc*. **89** (1990) 17.
7. J. ZHOU and S. BAHADUR, *Wear* **162–164** (1993) 285.
8. S. J. BENNISON, H. M. CHAN and B. R. LAWN, *J. Am. Ceram. Soc*. **72** (1989) 677.
9. N. A. TRAVITZKY, D. G. BRANDON and E. Y. GUTMANAS, *Mater. Sci. Eng.* **71** (1985) 77.
10. H. TOMASZEWSKI, *Ceram. Intl*. **14** (1988) 93.
11. H. P. KIRCHNER, "Strengthening of Ceramics" (Marcel Dekker, New York, 1979).
12. N. A. TRAVITZKY, D. G. BRANDON and E. Y. GUTMANAS, *Mater. Sci. Eng*. **71** (1985) 65.
13. W. A. ZDANIEWSKI and H. P. KIRCHNER, *Adv. Ceram. Mater*. **1** (1986) 99.
14. N. P. PADTURE, H. M. CHAN, B. R. LAWN and M. J. READEY, in "Tailored Interfaces in Composites, Vol. 170" (Materials Reserarch Society, Pittsburgh, 1990) p. 245.
15. N. P. PADTURE and H. M. CHAN, *J. Mater. Sci*. **29** (1991) 2711.
16. A. KRELL and P. BLANK, *Wear* **124** (1988) 327.
17. M. A. STOUGH, J. R. HELLMANN and J. C. CONWAY, *J. Mater. Sci*. **29** (1994) 3665.
18. B. A. LATELLA, PhD thesis, Curtin University, 1995.
19. B. A. LATELLA and B. H. O'CONNOR, *J. Mater. Sci*. **33** (1998) 877.
20. R. J. HILL and C. J. HOWARD, Australian Atomic Energy Commission (now ANSTO) Report no. M112, Lucas Heights Research Laboratories, NSW, Australia, 1986.
21. J. C. WURST and J. A. NELSON, *J. Am. Ceram. Soc*. **55** (1972) 109.
22. L. M. BRAUN, S. J. BENNISON and B. R. LAWN, *ibid.* **75** (1992) 3049.
23. B. R. LAWN, "Fracture of Brittle Solids" (Cambridge University Press, Cambridge, 1993).
24. G. R. ANSTIS, P. CHANTIKUL, D. B. MARSHALL and B. R. LAWN, *J. Am. Ceram. Soc.* **64** (1981) 533.
25. A. W. RUFF and L. K. IVES, *Wear* **35** (1975) 195.
26. S. J. BENNISON and B. R. LAWN, *Acta Metall*. **37** (1989) 2659.
27. R. F. COOK and D. H. ROACH, *J. Mater. Res.* **1** (1986) 589.
28. C. H. HSUEH and A. G. EVANS, *J. Am. Ceram. Soc.* **68** (1985) 120.
29. H. P. KIRCHNER, R. E. WALKER and D. R. PLATTS, *J. Appl. Phys*. **42** (1971) 3685.
30. D. B. MARSHALL, B. R. LAWN, H. P. KIRCHNER and R. M. GRUVER, *J. Am. Ceram. Soc.* **61** (1978) 271.
31. B. A. LATELLA and R. J. STEAD, in "Proceedings of the International Ceramic Conference Austceram 92, Vol. 1: Ceramics Adding the Value," edited by M. J. Bannister (CSIRO Publications, Melbourne, 1992) p. 400.
32. C. T. MORRISON, R. O. SCATTERGOOD and J. L. ROUTBORT, US Department of Energy Progress Report DOE-ER-4115-3, North Carolina State University, Raleigh, 1987, p. 124.
33. S. SRINIVASAN and R. O. SCATTERGOOD, *Wear* **142** (1991) 115.
34. J. L. ROUTBORT and R. O. SCATTERGOOD, in "Erosion of Ceramic Materials," edited by J. E. Ritter (Trans Tech Publications, Zurich, 1992) p. 23.
35. S. LATHABAI, *Mater. Forum* **19** (1995) 101.
36. R. W. DAVIDGE, "Mechanical Behaviour of Ceramics" (Cambridge University Press, Cambridge, 1979).
37. D. KOVAR and M. J. READEY, *J. Am. Ceram. Soc*. **77** (1994) 1928.
38. *Idem., ibid.* **79** (1996) 305.
39. A. G. EVANS, M. E. GULDEN and M. ROSENBLATT, *Proc. Roy. Soc. Lond*. **A361** (1978) 343.
40. S. M. WIEDERHORN and B. R. LAWN, *J. Am. Ceram. Soc*. **62** (1979) 66.
41. R. O. SCATTERGOOD and J. L. ROUTBORT, *ibid.* **66** (1983) C184.
42. S. WADA and N. WATANABE, *J. Ceram. Soc. Japan, Intl. Ed*. **95** (1987) 925.
43. B. R. LAWN, B. J. HOCKEY and S. M. WIEDERHORN, *J. Am. Ceram. Soc*. **63** (1980) 356.
44. C. A. POWELL-DOGAN, A. H. HEUER, M. J. READEY and K. MERRIAM, *ibid.* **74** (1991) 646.
45. D. KOVAR, private communication (1999).

§ In the above discussion the influence of T-curve behaviour, the magnitude of which is a function of grain size, has essentially been ignored but it obviously plays a critical role and is pertinent in ascertaining the wear resistance of the materials as has been shown in this and other studies. It is worthy to note that in work by Kovar [38] it was shown that broadening the grain size distribution did not influence the slope of the T-curve.

Received 25 June
and accepted 22 December 1999